Operational Atmospheric Landing Guidance for Reusable Rockets

Marco Sagliano *, Stefano Farì[†], José Máces Hernández[‡], Francesco Marchetti [§], Henrik Harms [¶], Ansgar Heidecker [‖]José Redondo Gutierrez **, David Seelbinder[††] and Etienne Dumont[‡‡]
German Aerospace Center, Bremen, Germany, 28359

Svenja Woicke [§§]
OHB System AG

This work focuses on the development and the analysis of atmospheric landing guidance solutions for reusable rockets in the context of the CALLISTO project, a first-stage demonstrator jointly developed by DLR, JAXA, and CNES. The most recent developments of the scenario are discussed, with a special emphasis on the handling of a complex operational constraint arising from the physical limitations of the actuators in use. We propose a simple technique to avoid multi-phase modeling of the landing guidance problem due to the aforementioned limitations, and show some numerical results obtained for one of the reference test flights of CALLISTO.

I. Introduction

Reusable rockets are currently the focus of space technological development over three different continents. The United States' private company SpaceX regularly performs more than one launch per week with its highly successful Falcon 9 rockets (in 2024 only they had 120 launches at the moment we write these words) and keeps leading the way with 3 Starship launches completed last year [1]. The new flagship rocket of Elon Musk's company continues to introduce innovations, such as the *Mechazilla chopsticks mechanism* to grasp the super-booster on the fly [2].

The Chinese startup Landspace, with its Zhuque-3 rocket, able to perform an entire vertical take-off and landing flight sequence, is also making significant steps towards the development of an operational reusable rocket [3]. In Japan, previous efforts can be traced back into the experimental flight tests of the Japan Aerospace Exploration Agency (JAXA) RVT rocket [4]. In Europe, although on a different scale, relevant tests were made by the German Aerospace Center (DLR) with the EAGLE demonstrator [5], by the French National Center for Space Studies (CNES) with the FROG vehicle [6], as well as by the Romanian National Institute for Aerospace Research "Elie Carafoli" (INCAS), in cooperation with the European Space Agency (ESA), leading to the development of the DTV lander [7].

Given the economic and strategic importance of the specific market at stake, that is, the launchers segments and all the derived services, the efforts towards the development of reusable rocket technologies constantly gained momentum. This was especially true from the point of view of one of the key subsystems, namely the Guidance, Navigation, and Control (GNC), which also experienced an increase in the number of studies, especially in the context of descent and landing guidance and control solutions (e.g., [8–14]), as well as in the development of dedicated numerical benchmarks (e.g., [15, 16]) for further acceleration of the related algorithmic development.

With the objective to move towards more operative capabilities, the space agencies of Germany, France, and Japan strategically decided to share their efforts, know-how, and resources and develop a first-stage reusable demonstrator. The resulting project, CALLISTO (Cooperative Action Leading to Launcher Innovation in Stage Tossback Operations), is now in an advanced stage of design, and it will perform a series of test flights of increasing complexity at the Guiana Space Center (GSC) [17].

*GNC Senior Researcher, Department of Guidance, Navigation, and Control, AIAA Senior Member
[†]PhD Candidate, Department of Guidance, Navigation, and Control
[‡]GNC Researcher, Department of Guidance, Navigation, and Control
[§]GNC Researcher, Department of Guidance, Navigation, and Control
[¶]GNC Researcher, Department of Guidance, Navigation, and Control
[‖]CALLISTO GNC System Engineer, Department of Guidance, Navigation, and Control
**CALLISTO GNC Project Manager
[††]G&C Group Head, Department of Guidance, Navigation, and Control
[‡‡]CALLISTO Project Manager
[§§]Former CALLISTO GNC Project Manager, now Project Chief Engineer

One of the key technologies of CALLISTO is of course represented by the GNC system, in particular the landing guidance. In the literature there are many studies available that deal with the landing guidance problem formulation, both in vacuum [18–20], and in the presence of atmospheric and aerodynamic effects [8, 21, 22]. A further difficulty arises when the engine properties have to be taken into account. Re-ignition of the engine during the descent and landing phase implies in practice an idle mode and a finite transient time before the engine is 100% operative. Several techniques to deal with more realistic engine effects were proposed in recent years. For instance, thrust-rate limiters [23], multipulse modeling [24], and, more recently, explicit parametrization of thrust profiles [25]. Still, to the best of our knowledge, the explicit inclusion of the idle and the transient regimes of the engine was never treated to date. This is even truer in the context of solutions relying on convex optimization, a methodology largely employed in countless space applications in the last years [9, 10, 26–34]. The inclusion of such effects would naturally lean towards an intrinsically multiphase, non-convex formulation to reflect the behavior of idle and transient modes in the generated solutions. However, to keep the computational complexity level as low as possible, we propose a simple alternative formulation that embeds the feature of the multiphase behavior into a single-phase subproblem, that is solved with a Sequential Pseudospectral Convex Programming (SPCP) approach [8, 35].

While in our previous work we focused on the evolution of the different studies performed to frame the landing guidance problem for the CALLISTO demo flight [35] (now renamed `Test Flight E`) in this context we revisit the problem to consider a realistic engine behavior in the formulation. Specifically, due to project timeline constraints, we provide some further preliminary results obtained for `Test Flight D`.

The structure of the paper is the following: in Sec. II we provide a brief description of the vehicle and the mission scenario. Section III focuses on the description of the Optimal Control Problem (OCP) representing the Powered Atmospheric Landing Guidance (PALG) problem for the CALLISTO rocket, and on the multi-phase into single-phase embedding proposed to deal with the engine model in use for CALLISTO. Section IV contains some of the preliminary results obtained for `Test Flight D`. Finally, some concluding remarks about this work and the future related activities are detailed in Sec. V.

II. Vehicle and Mission

While in [35] we put the emphasis on the `Test Flight E` (aka the *Demo* flight) in this section we provide an overview of the mission scenario for the current test flight under analysis, that is, `Test Flight D`. In addition, we provide a description of the major changes to the modeling of the CALLISTO rocket.

A. Rocket Modeling

The first-stage CALLISTO demonstrator is a 40-kN class rocket, with a throttle capability between 40% and 110% of the nominal maximum thrust that the Liquid Oyxgen (LOX) - Liquid Hydrogen (LH2) engine can generate. An impression of the rocket can be seen in Fig. 1a. During the powered phases (that is, ascent and landing) of the flight experiments, a gimballing system provides pitch and yaw control capability. A set of eight reaction control system (RCS) thrusters, mounted close to the nose of the rocket, provides roll control capabilities [36]. In addition, the rocket is equipped with four aerodynamic steerable fins, mounted on top of the vehicle. Once that they are deployed, they are utilized to aerodynamically control the vehicle during the unpowered phases. A combination of RCS and aerodynamic fins is in use during the powered landing phase too. Therefore, except for the translational motion around the apogee, during which the engine is off, and the dynamic pressure too low to aerodynamically control the rocket, the system is fully controllable throughout the rest of the mission.

Since we focus on the landing phase, characterized by a large mass depletion, the vehicle experiences a significant variation of its center of mass CoM. Therefore, this effect was included by using a simple look-up table, which outputs the expected CoM depending on the estimated current value of the mass m. Note that in this context we neglect the mass variation due to the use of the RCS thrusters. The dependency is therefore schematized simply as

$$CoM = CoM(m) \tag{1}$$

while, from the point of the aerodynamic behavior of the rocket, the total angle of attack α_T and the windward meridian angle Φ_T [38, 39], depicted in Fig. 1b, were adopted to generate the corresponding look-up tables expressing the aerodynamic coefficients as a function not only of these two angles, but also of the Mach number M, and the four fin

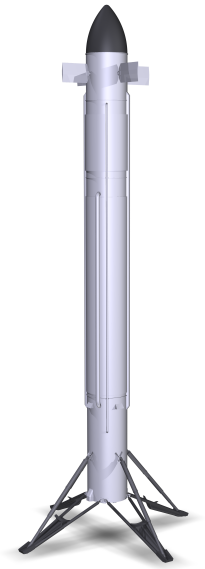

(a) CALLISTO experimental vehicle.

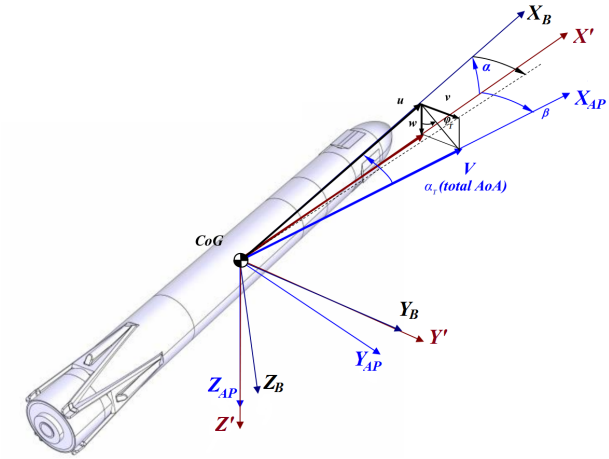

(b) Representation of the aerodynamic angles: Total Angle of attack α_T, windward meridian angle ϕ_T (used for the AEDB computations), angle of attack α and sideslip angle β (used for trajectory optimization), together with the Body axes and the Airpath (AP) axes [37].

Fig. 1 Vehicle overview: (a) CALLISTO rocket, (b) Aerodynamic angles of the CALLISTO rocket.

deflections δ_1,δ_2,δ_3,δ_4 through extensive computational fluid dynamics (CFD) simulations [40].

$$\mathbf{C}^{aero}_{BODY} = \begin{bmatrix} C^{aero}_{BODY,x}(M, \alpha_T, \Phi_T, \delta_1, \delta_2, \delta_3, \delta_4) \\ C^{aero}_{BODY,y}(M, \alpha_T, \Phi_T, \delta_1, \delta_2, \delta_3, \delta_4) \\ C^{aero}_{BODY,z}(M, \alpha_T, \Phi_T, \delta_1, \delta_2, \delta_3, \delta_4) \end{bmatrix} \tag{2}$$

The aerodynamic force in body coordinates can therefore be computed as follows.

$$\mathbf{F}^{aero}_{BODY,i} = \tfrac{1}{2}\rho V^2 S \mathbf{C}^{aero}_{BODY,i} \quad , \quad i = x, y, z \tag{3}$$

In Eq. (3) the reference surface S is assumed to be equal to 0.95 m, while the term ρ represents the atmospheric density, which is modeled as a look-up table built upon a series of in-situ measurements as a function of the geodetic altitude.

$$\rho = \rho(h)$$

As we emphasized in past studies as well [8, 35], the previous equations show that no strong simplifications (i.e., an exponential atmospheric profile) are required with the proposed method.

B. Mission Scenario

A series of flights of increasing complexity will take place at the Guiana Space Center, the European Spaceport in French Guiana. This flight campaign will provide valuable real data on the behavior of the system during the active flights that will allow to refine models and to verify the performance of the different subsystems. In addition, it will lead to key information on the level of refurbishment of several components required between two consecutive flights. At the same time, these tests will provide first-hand data to all the partners to further enhance the knowledge of reusable technologies and some of the related critical technologies, especially within the GNC domain. In this paper we analyze the `Test Flight D`: this is a Return-to-Launch-Site (RTLS) scenario, but with a slightly lower altitude if compared with the `Test Flight E` presented in [35]. The sequence is however, very similar in the two flights. Once that, during the aerodynamic descent, the rocket reaches a specific predefined (test-flight-dependent) altitude, the re-ignition command is issued by the Mission and Vehicle Manager (MVM), leading to the formal beginning of the Powered Atmospheric Landing sequence. This phase is completed once that the rocket safely touches the ground with its legs. The engine is then shutdown for the second and last time, leading to the end of the test flight. The entire reference trajectory is depicted in Fig. 2, together with the axes representing the Downrange, Crossrange, and Altitude direction (in rgb convention), centered at the prescribed landing location.

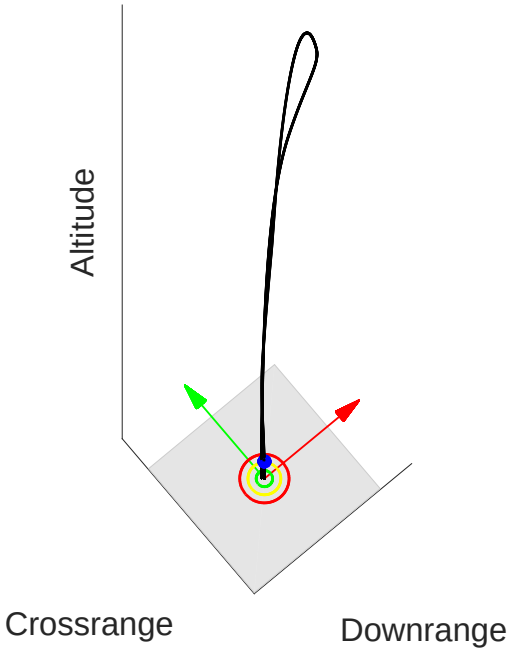

Fig. 2 Return-to-Launch-Site mission profile (`Test Flight D`).

III. Powered Atmospheric Landing Guidance Problem

In this section we formulate the PALG problem for the `Test Flight D`. This formulation heavily relies on the previous studies with two key differences: the idle and transient mode are taken into account, while for `Test Flight D` there is no specific final-thrust requirement, as it was instead the case of `Test Flight E`. This difference leads to a potential way to further improve computationally the guidance method for the specific test flight we consider here, as we will see.

A. Baseline Formulation

The baseline optimal control problem for the atmospheric landing of CALLISTO can be formulated as follows: we want to minimize the fuel consumption while heavily penalizing the excessive use of aerodynamic angles to avoid the presence of large aerodynamic torques to be compensated for. In addition, we want to land at the prescribed position if this is possible. But, in case the position error at the beginning of the powered atmospheric landing sequence is too large, the priority should instead go to the minimizing the final position error. These requirements translate into the following cost function,

$$\underset{\mathbf{u},t_F}{\text{minimize}}\ J = \omega_{DC} s_{DC} + \int_{t_0}^{t_F} \left(T_{cmd} + \omega_\alpha u_\alpha^2 + \omega_\beta u_\beta^2 + \omega_{\epsilon_1} u_{\epsilon_1}^2 + \omega_{\epsilon_2} u_{\epsilon_2}^2 \right) dt \tag{4}$$

where s_{DC} is a slack variable introduced to penalize the final horizontal position error, through the imposition of the following conic constraint.

$$(D(t_F), C(t_F), s_{DC}) \in \mathcal{K}^3 \tag{5}$$

For this problem the controls are

$$\mathbf{u} \triangleq \left[T_{cmd},\ u_\alpha,\ u_\beta,\ u_{\epsilon_1},\ u_{\epsilon_2} \right]^T \tag{6}$$

with T_{cmd} that is the commanded thrust value, u_α and u_β the rates of the angle of attack α and the sideslip β, while u_{ϵ_1} and u_{ϵ_2} are the rates of the thrust vector control (TVC) deflections ϵ_1 and ϵ_2, included to avoid sudden jumps in the tilting of the engine. The weights ω_{DC} and ω_i, with $i = \alpha,\ \beta,\ \epsilon_1,\ \epsilon_2$, measure the relative importance of the final error, represented by the slack variable s_{DC} and the penalization of the aerodynamic-propulsive controls defined in Eq. (6) with respect to the fuel consumption, (represented by the minimization of the vacuum thrust T_{vac}, here approximated with the commanded atmospheric thrust T_{cmd}). For the `Test Flight D` we adopted $\omega_{DC} = 10^4$, and a common value of 10^3 for the other four weights appearing in the cost function of Eq. (4).

The three-degree-of-freedom (3-DoF) equations of motion, expressed with respect to the *Downrange-Crossrange-Altitude (DCA)* reference frame depicted in Fig. 2, are given by

$$\begin{aligned}
\dot{\mathbf{r}} &= \mathbf{v} \\
\dot{\mathbf{v}} &= \mathbf{a}^{grav} + \mathbf{a}^{thr} + \mathbf{a}^{aero} + \mathbf{a}^{fict} \\
\dot{m} &= -\frac{T_{vac}}{I_{sp} g_0} \\
\dot{\alpha} &= u_\alpha \\
\dot{\beta} &= u_\beta \\
\dot{\epsilon_1} &= u_{\epsilon_1} \\
\dot{\epsilon_2} &= u_{\epsilon_2}
\end{aligned} \tag{7}$$

Details on the computation of the different terms are provided in [35], and therefore omitted here to avoid repetitions. The states adopted for this representation are consequently given by

$$\mathbf{x} \triangleq \left[\mathbf{r}^T,\ \mathbf{v}^T,\ m,\ \alpha,\ \beta,\ \epsilon_1,\ \epsilon_2 \right]^T \tag{8}$$

with $\mathbf{r}$ and $\mathbf{v}$ representing the position and the velocity vectors of the CoM expressed in the DCA reference frame. The boundary conditions for the PALG problem are given by

$$\mathbf{x}^+(t_0) = \mathbf{x}_0^+, \quad \mathbf{x}^*(t_F) = \mathbf{x}_F^* \tag{9}$$

with $\mathbf{x}^+$ including position, velocity, mass, angle of attack and sideslip angle (while the TVC angles are left free), whereas $\mathbf{x}^*$ accounts only for the final values of altitude, velocity vector, angle of attack, and sideslip angle (to ensure a

correct vertical landing). Other constraint to be taken into account are the box constraints associated with some of the states,

$$\begin{array}{rcccl} m_L & \leq & m & \leq & m_U \\ \alpha_L & \leq & \alpha & \leq & \alpha_U \\ \beta_L & \leq & \beta & \leq & \beta_U \\ \epsilon_{1,L} & \leq & \epsilon_1 & \leq & \epsilon_{1,U} \\ \epsilon_{2,L} & \leq & \epsilon_2 & \leq & \epsilon_{2,U} \end{array} \tag{10}$$

as well as the controls,

$$\begin{array}{rcl} T_{min} & \leq & T_{cmd} \\ T_{cmd} & \leq & T_{max} \\ |u_\alpha| & \leq & \dot{\alpha}_{max} \\ |u_\beta| & \leq & \dot{\beta}_{max} \\ |u_{\epsilon_1}| & \leq & \dot{\epsilon}_{1max} \\ |u_{\epsilon_2}| & \leq & \dot{\epsilon}_{2max} \end{array} \tag{11}$$

with T_{min} and T_{max} corresponding to 40% and 110% of the nominal maximum value of the thrust. The minimum and maximum values for the angle of attack and the sideslip angles are given by $[170,\ 190]$ deg and $[-10,\ 10]$ deg, respectively, while all the rates are bounded to be within $[-5,\ 5]$ deg/s. The lower bound for the mass, m_L is clearly represented by the dry mass m_{dry} of the vehicle, while the upper bound is the wet mass m_{wet} of the rocket. Note that this last inequality is never active, since the mass can only diminish, and the initial value of the mass at the power descent and landing initiation is already clearly lower than m_{wet}. The problem represented by the minimization of Eq. (4), subject to Eqs. (5)-(11) is the baseline problem we want to solve. However, nothing has been mentioned yet about the treatment of the idle and transient regimes of the engine. This is the focus of the next section.

B. Operational Formulation

In the previous section we defined the range for the commanded thrust to be between 40% and 110% of the maximum nominal thrust of CALLISTO. While for guidance preliminary prototyping it is fine to consider the engine as capable of immediately provide a thrust at least equal to T_{min}, this is not what happens in reality: once that the re-ignition command is issued by the Mission Vehicle Management system, the engine enters the *idle mode*, meaning that the thrust from 0 newton will rise to a small, constant thrust for some seconds. The duration is typically characterized by experiments, and varies from engine to engine. During this phase the specific impulse is not constant either, and this aspect needs to be taken into account as well. Finally, there is a *transient* behavior to consider, that has a non-negligible effect on the trajectory, since the rocket will obviously not slow down as during a full-propelled phase. Only after a finite interval of time the thrust will grow until reaching the operative range $[T_{min},\ T_{max}]$. This behavior makes the problem strongly non-convex, due to the physical separation of the thrust subdomains, as visible in Fig. 3. The natural solution for this class of problems would be the introduction of a multiphase framework, with the idle, the transient and the operational modes represented by different phases. However, from the practical point of view, this approach complicates the design: having a multi-phase approach is not viable, due to complexity it brings to both the transcription and the solving process, which must be as fast as possible.

The following solution was therefore adopted to circumvent these limitations while keeping the formulation a single-phase optimal control problem. First, we introduce a new state ξ, which is nothing else than the time. Its differential equation will therefore be simply given by

$$\dot{\xi} = 1 \tag{12}$$

The inclusion of time as a state has the purpose of replacing the way the thrust is injected into the problem. In fact, the thrust will be now computed as

$$T_{atmo} = g(\xi, T_{cmd}) \tag{13}$$

where the dependency with respect to ξ, i.e., the time, allows to model the idle phase and the transient in a more realistic way, and to make the inclusion of such complex model compatible with a single-phase formulation of the sequential convex approach. A visual representation of the transformation is visible in Figs. 4a and 4b. In the former two time-response plots of the actual engine model for a given command (e.g., 40% or 110%) are provided. Note that

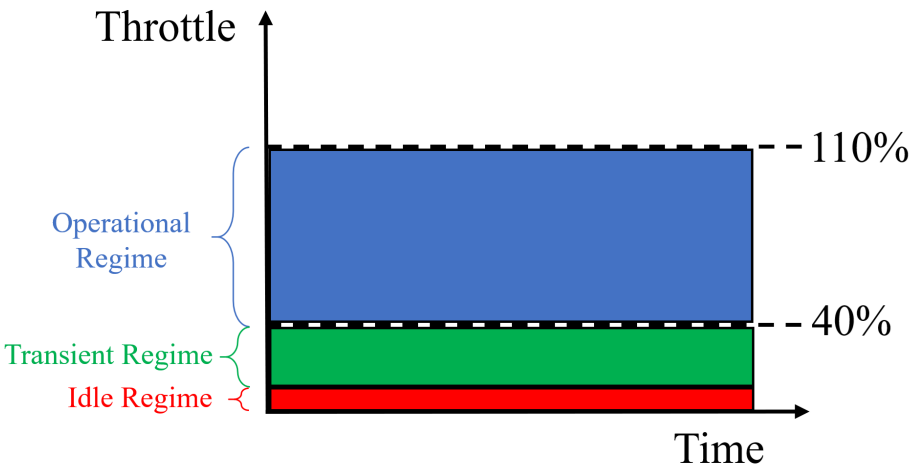

Fig. 3 Thrust domain representing idle, transient and operational regime.

the idle phase is already quite complex, with an initial thrust equal to 0 kN, which goes up to a small thrust value in a finite time, and remains constant for another small time interval. Afterwards, the transient to the commanded value is visible. One can also see how the response is slightly slower when the commanded thrust is smaller, and quicker for high values of thrust. In addition, there is a strong nonlinearity for the 40% command visible at t = 0.25, which cannot be easily captured by simple representations, such as 1^{st} or 2^{nd}-order transfer functions. By considering the time as an additional independent variable, we obtain the plot of Fig. 4b.

The advantage of this approach is simple: the actual thrust generation becomes a 2-D look-up table, function of the commanded thrust T_{cmd}, which continues to be defined between 40% and 110%. However, the second variable allows to correctly provide the time-dependency, allowing for an accurate inclusion of both idle and transient with no modifications to the Sequential Convex Programming approach in use. Although very simple, this approach allows to embed time-dependent effects into any standard Sequential Convex framework, thus avoiding the use of dedicated phases and the corresponding multiphase formulation. That is why we refer to it as *multiphase into single-phase embedding*. The optimal control problem highlighted in the previous section then is augmented with a further differential equation, given by Eq. (12), by the inclusion of the model of Eq. (13), as well as by the trivial initial condition $\xi(t_0) = 0$.

C. Problem Transcription

The transcription of the problem into its finite-dimensional counterpart is performed with our Sequential Pseudospectral Convex Programming (SPCP) approach, already detailed in previous works ([8, 35]). The corresponding details are therefore not described here to avoid tedious repetitions, and we encourage the interested reader to refer to our previous works instead. What is just worth to be mentioned here is that all the numerical cases were generated by considering only one segment with 25 collocation nodes. This choice was justified by the reduced time of flight that we experience with `Test Flight D`.

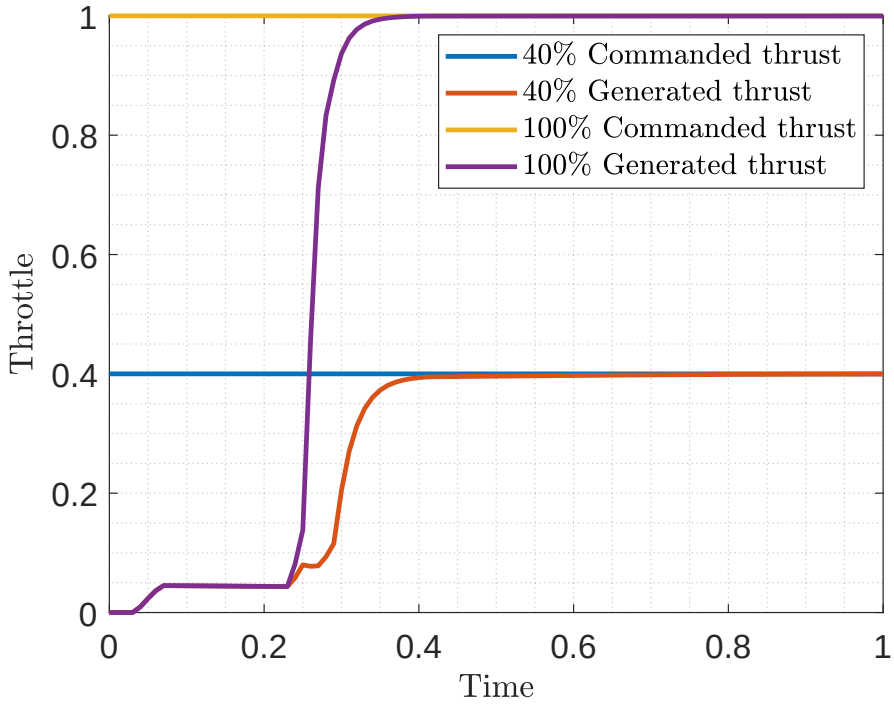

(a) Time-response of thrust model.

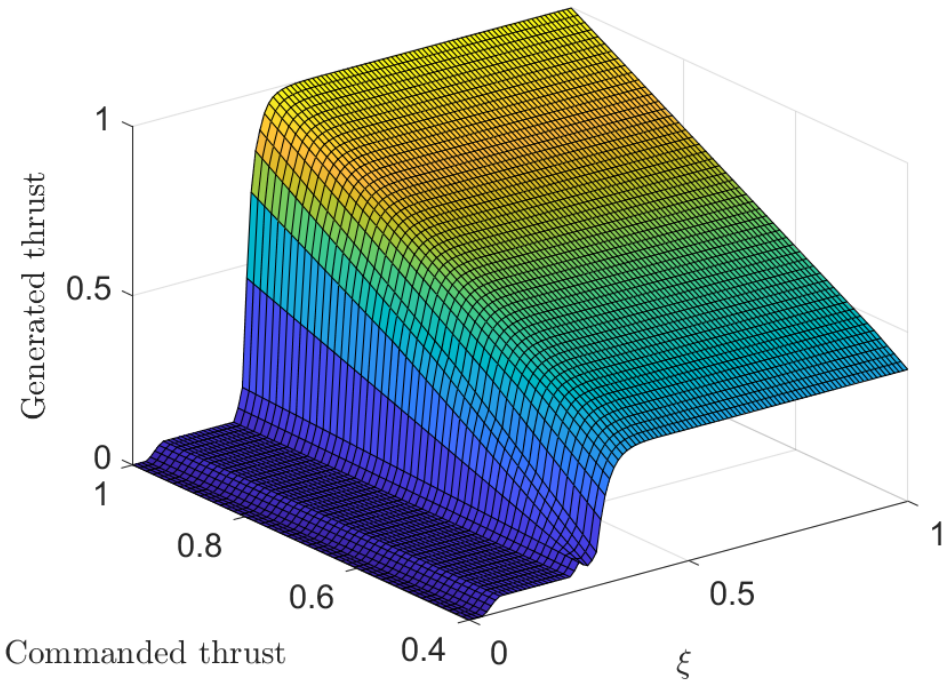

(b) Augmented model of thrust.

Fig. 4 Augmentation of thrust model for multi-phase embedding.

IV. Numerical Results

In this section we first provide some results obtained for the nominal scenario. Then, we present a series of results coming from a mini-Monte-Carlo campaign (100 cases) that we run to initially assess the robustness of the PALG landing guidance scheme developed. All the results were generated with Matlab 2021b, running on a CPU i7, with 16GB of RAM. The convex solver in use is ECOS [41]. All the plots are non-dimensional. The reference length and speed were the initial altitude and vertical speed at the moment of beginning the landing sequence, while the initial mass of the nominal scenario was used as reference mass value.

A. Nominal case

The nominal results obtained are depicted in Figs. 5-9. First, we can observe the resulting trajectory in Fig. 5, with its 2-D projections in Fig. 6. The trajectory correctly lands at the prescribed position, exhibiting reduced side-motion. The penalization of the aerodynamic angles, and the TVC angles is visible in Fig. 7, where we can see an angle of attack variation of about 0.5 deg, while the sideslip angle exhibits a maximum oscillation of about 4 deg. The TVC angles are quite limited, with maximum feedforward deflections in absolute terms equal to 0.5 and 0.3 deg, respectively. Figure 8 shows the corresponding rates. All the values, in virtue of the penalization (in quadratic sense) in Eq. (4) show quite limited values. Finally, the most interesting plot is the one in Fig. 9. We see the evolution of the non-dimensional profiles of altitude, speed and mass. In addition, we can observe how the proposed method handles the idle and transient phases: while the commanded value is defined between 40% and 110%, as expected, the embedding on the engine behavior leads to correctly include the idle (red area) and the transient mode (green area) in the solution, leading to more realistic results compared to the case where these effects are simply ignored.

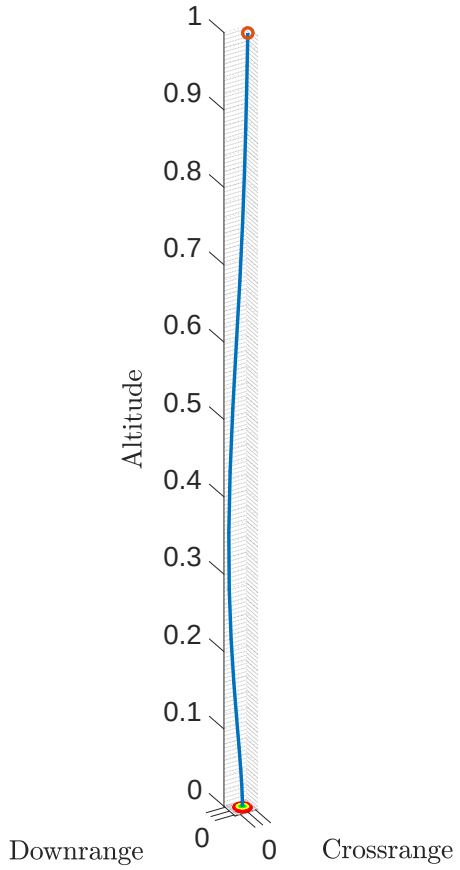

Fig. 5 Nominal trajectory in DCA coordinates.

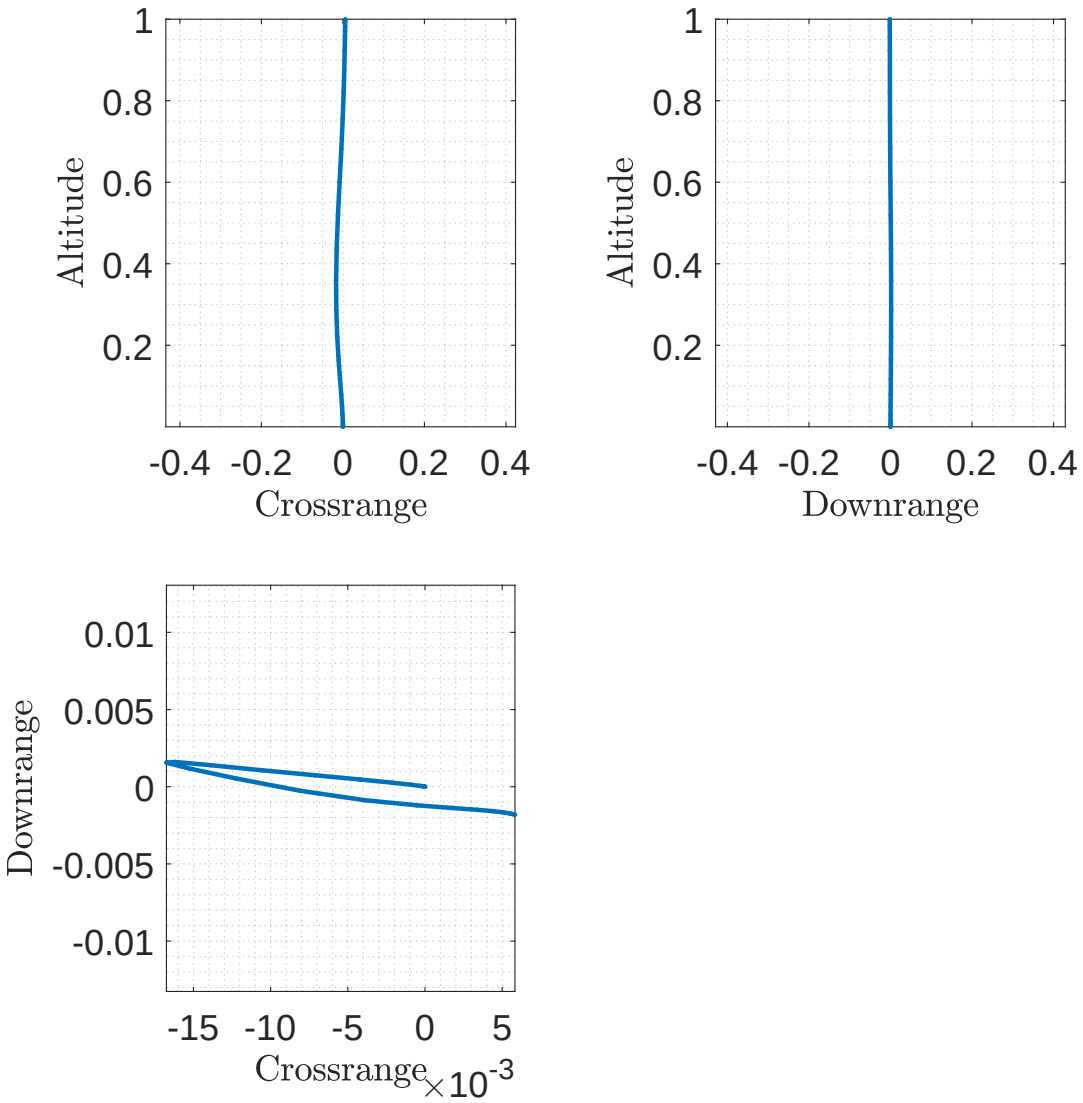

Fig. 6 Projections of the nominal trajectory in DCA coordinates.

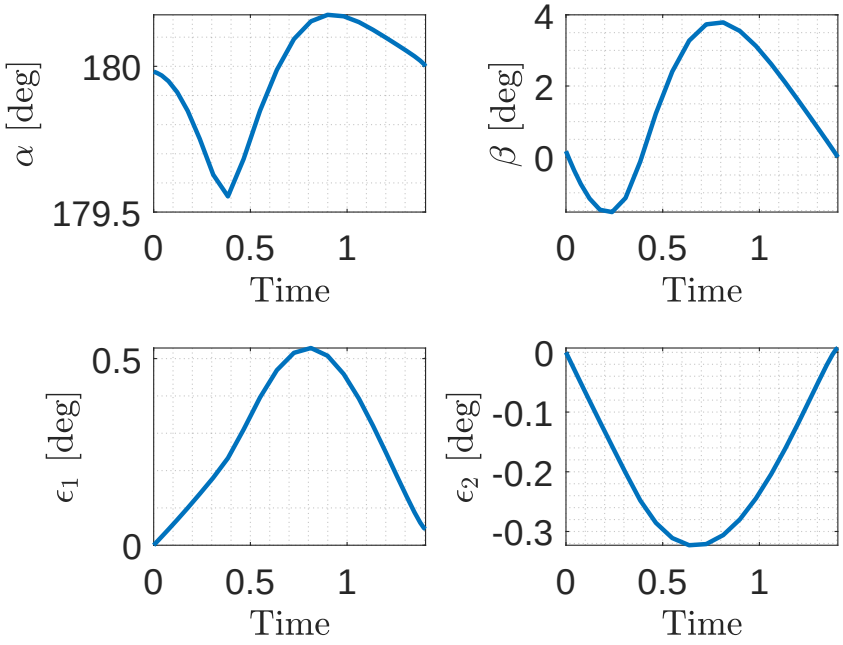

Fig. 7 Aerodynamic and propulsive angles.

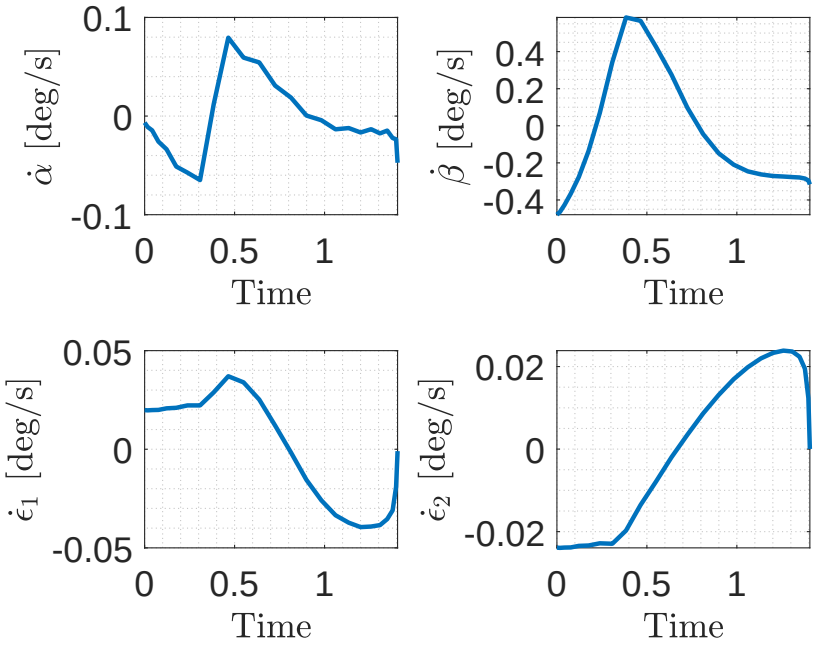

Fig. 8 Aerodynamic and propulsive angular rates.

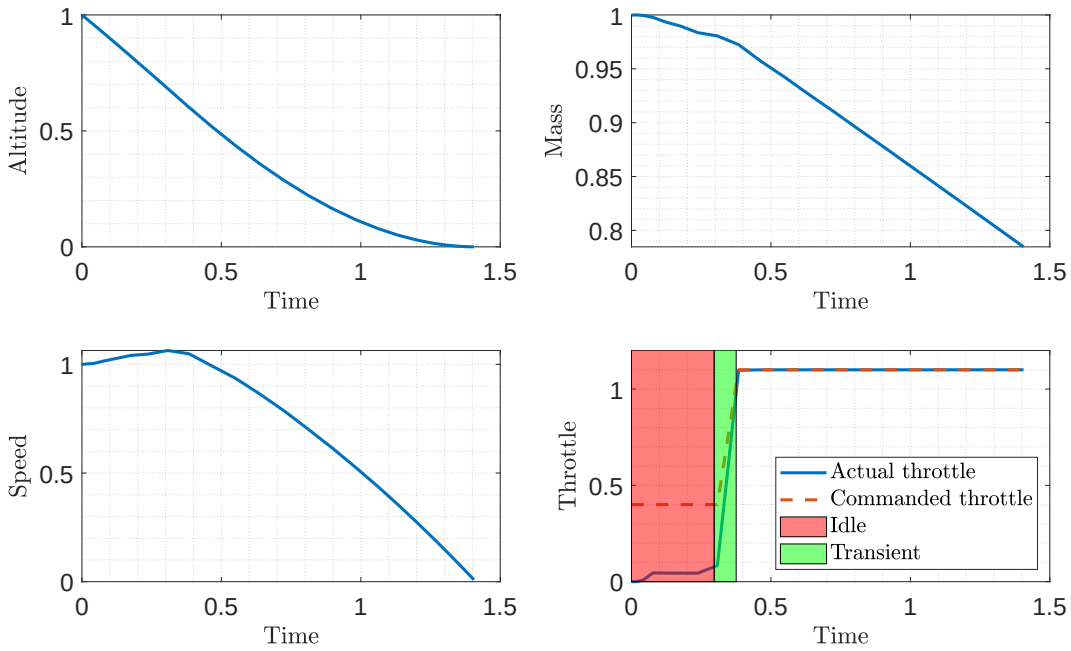

Fig. 9 Altitude, speed, mass and throttle profiles.

B. Monte-Carlo results

In this section we show some first results associated with dispersed initial conditions. These results were generated by considering an initial horizontal position error of 100 m along the crossrange and the downrange directions, while the three components of the velocity vector had an error up to $\pm 10\ \mathrm{m\,s^{-1}}$. In addition, we considered a dispersion of the initial mass up to ± 15 kg. All these values were assumed uniformly distributed. Given the limited number of cases (100 runs) it is improper to refer to them as a Monte-Carlo campaign. Nonetheless, these cases provide some first hints about the robustness and convergence properties of the algorithm. Results are depicted in Figs. 10 through 14. First, we see in Fig. 10 that all the trajectory converge to the prescribed final position. The behavior of the algorithm is rather consistent, with all the trajectories showing a similar trend, although this might change when larger dispersions are considered. We can also observe in the downrange-crossrange evolution (bottom-left plot of Fig. 11), that, depending on the combination of position and velocity, the rocket overshoots the target position while maneuvering along the crossrange direction, before inverting the downrange motion to meet the target conditions. The effect is nevertheless quite limited. Figures 12 and 13 show the aerodynamic and propulsive angles, as well as their corresponding rates. Although clearly larger than for the nominal conditions, their values are well within the prescribed boundaries, showing a good degree of safety for the proposed scheme. The maximum angle-of-attack variation with respect to the vertical landing conditions (that is, 180 deg), are less than 1.5 deg, and about 6 deg for the sideslip angle. The TVC angles never reach 1 deg. All the rates are also well within their bounds. Finally, Fig. 14 shows the altitude, speed and mass profiles, together with the actual engine throttle. As expected, there is consistency of behavior in all the cases. Moreover, we can observe that, at least for `Test Flight D`, the scenario would correspond to the classical *min-max*optimal control structure, in this case, due to the engine properties, replaced by *idle-transient-max*. This behavior translates into having all the thrust profiles practically identical, with the only difference coming from the final times, which vary from case to case. However, this observation leads to the possible simplification of the scheme where the thrust could be completely removed as a control from the problem, and provided as a look-up table as explained in Sec. III.B. This approach could further accelerate the computation of a solution, and is an option to be explored in the future.

Finally, Table 1 shows a snippet of the results of the 100 cases with details about the convergence, the horizontal position error at touchdown, and the virtual slack obtained for each specific case. Specifically, the downrange and crossrange errors (columns 2 and 3) show that all the cases were in practice able to reach the prescribed landing position. The maximum virtual slack in column 4 gives a measure of the residual use of virtual controls (see [35], Eq. 53 for details) within the discretized dynamics of the system. All the values are in the order of $[10^{-11},\ 10^{-9}]$, confirming the dynamical feasibility of the computed solutions. From the point of view of the convergence, the mean CPU time is 0.8 s, with a standard deviation of 0.16 s. The mean number of iterations is 5.54, with a standard deviation of 0.52. The maximum number of iterations observed is 7, while the maximum CPU time was 1.69 s. While these figures do not tell much about the time required to run the algorithm on the onboard processor, they are a promising starting point, since they are all computed with a cold start, and further acceleration can come from a proper initialization strategy and from an improvement of the implementation efficiency.

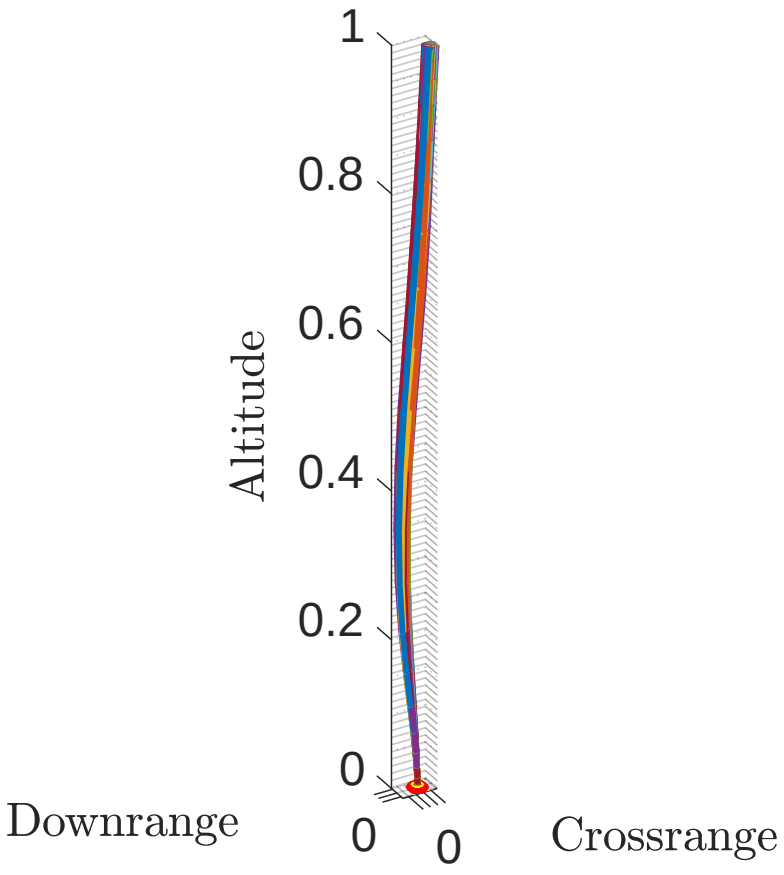

Fig. 10 Dispersed trajectories - 100 cases.

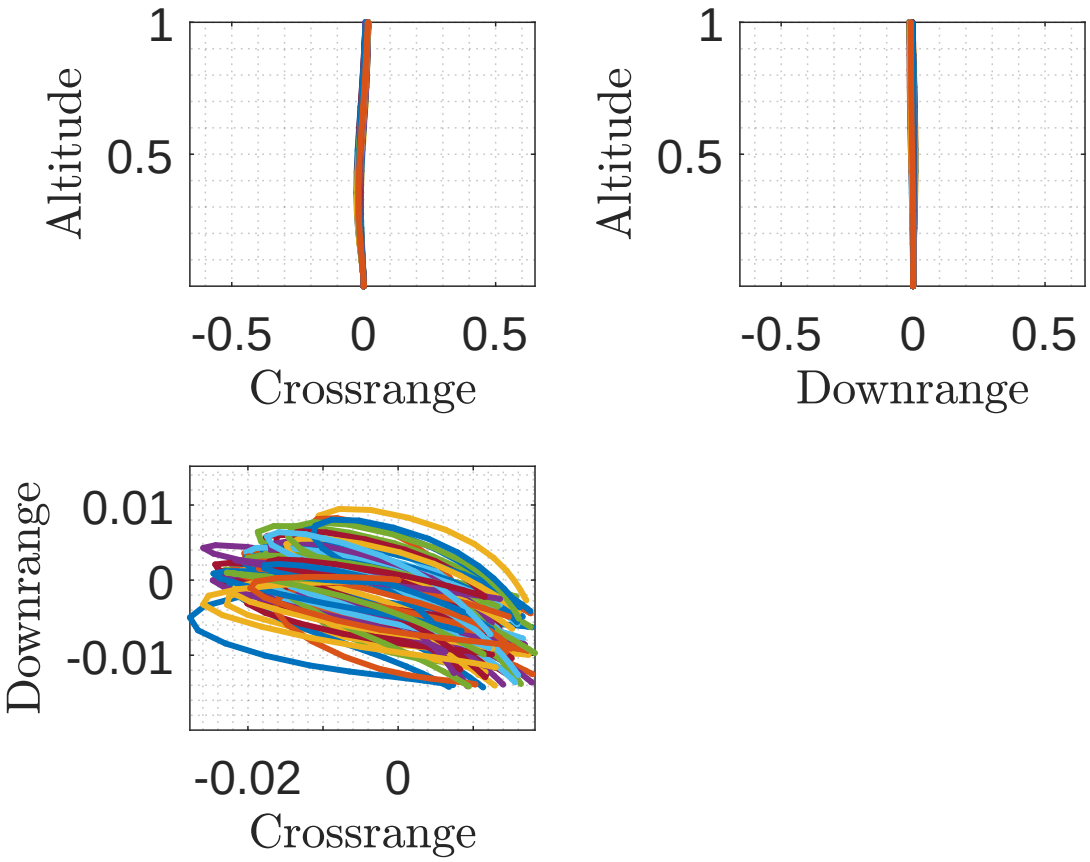

Fig. 11 Projection of dispersed trajectories - 100 cases.

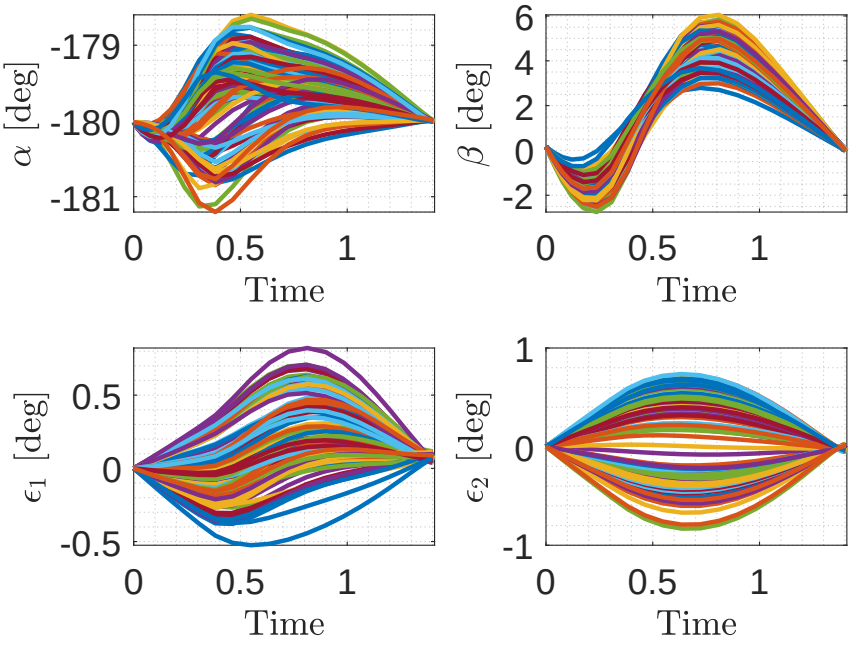

Fig. 12 Aerodynamic and propulsive angles - 100 cases.

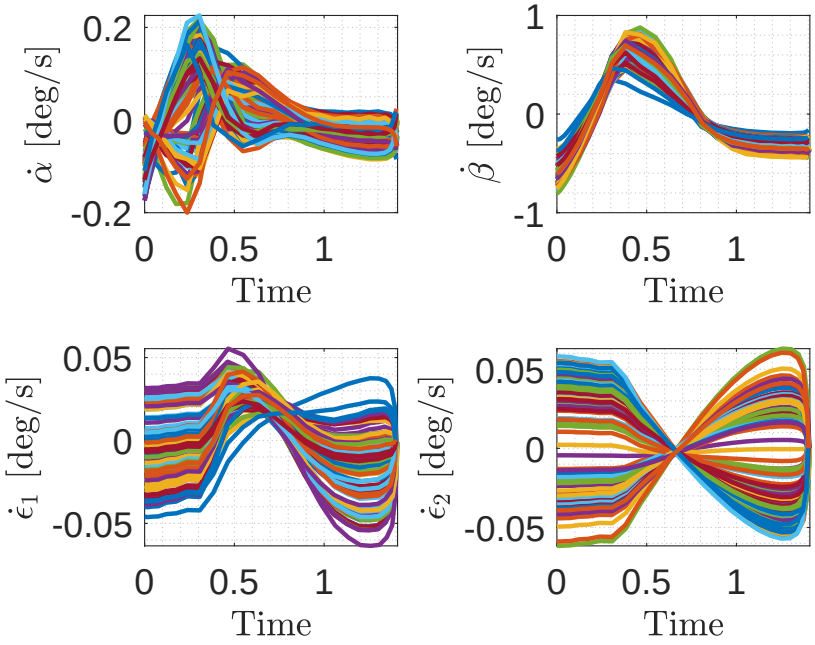

Fig. 13 Aerodynamic and propulsive angular rates - 100 cases.

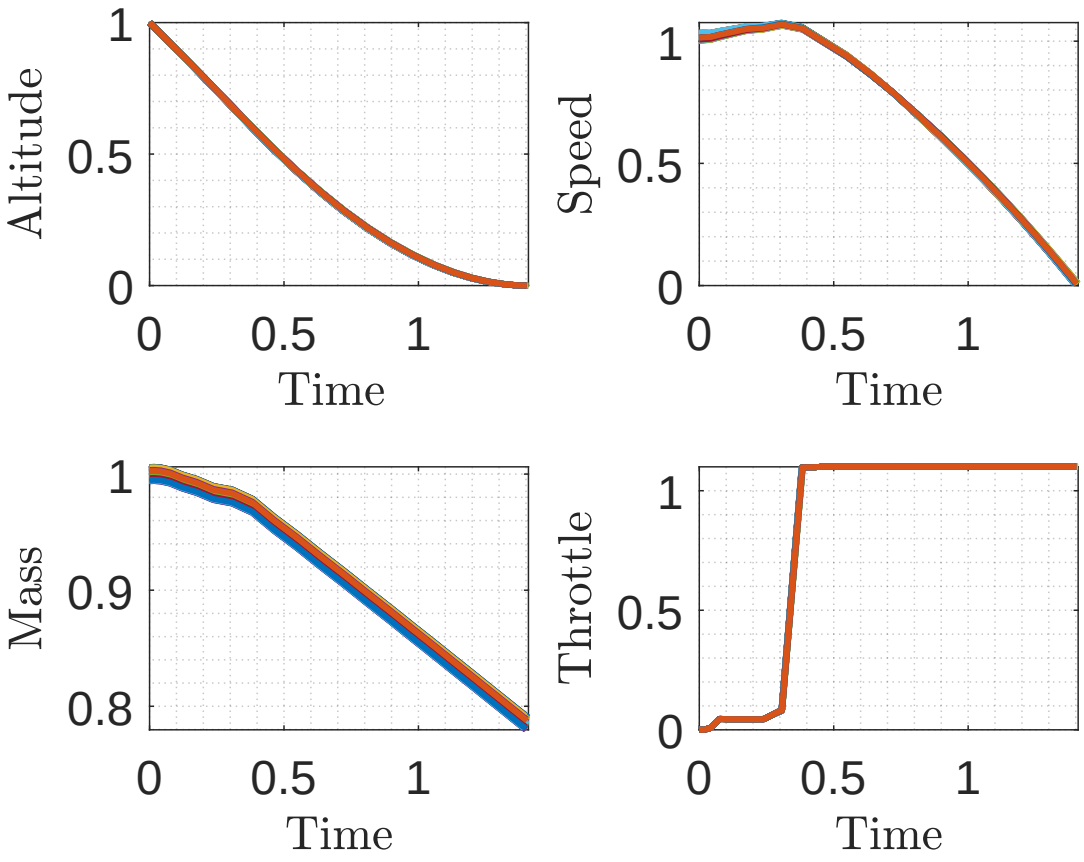

Fig. 14 Altitude, speed, mass and throttle profiles - 100 cases.

Table 1 Snippet of performance observed within the mini-MC.

Id	Downrange Error	Crossrange Error	Max. Virtual Slack	Iterations	CPU Time	Successful
-	-	-	-	-	[s]	
1	1.914e-10	-2.548e-11	1.4468e-10	6	1.5745	Yes
2	8.1311e-11	1.3984e-10	1.4226e-10	5	0.62531	Yes
3	1.1061e-10	2.4488e-10	2.1911e-10	5	0.66397	Yes
4	5.0635e-10	7.0654e-10	4.0218e-10	5	0.62072	Yes
5	-1.5926e-09	1.5846e-09	2.3036e-09	6	1.6976	Yes
6	2.6101e-10	2.409e-10	3.3403e-10	6	0.78718	Yes
7	-9.4897e-11	3.1948e-10	2.9881e-10	5	0.69682	Yes
8	2.3171e-10	-4.4737e-10	2.305e-10	6	0.84101	Yes
9	-1.9195e-11	1.701e-10	2.0186e-10	6	0.86708	Yes
10	9.5687e-10	-1.2326e-10	1.6823e-09	5	0.69003	Yes
11	2.334e-10	-5.5147e-11	7.9916e-10	6	0.77439	Yes
12	5.7487e-11	-4.6105e-11	2.7414e-10	5	0.74144	Yes
13	2.8104e-11	-3.3342e-11	1.4055e-10	5	0.63775	Yes
14	6.6991e-10	6.1716e-10	1.1377e-09	5	0.96998	Yes
15	-1.4545e-09	3.9568e-09	3.5327e-09	7	0.96111	Yes
16	7.991e-11	4.2272e-10	5.1533e-10	6	0.77543	Yes
17	5.6115e-10	6.9429e-10	1.5726e-09	6	1.011	Yes
18	-5.4267e-11	-1.0203e-13	2.3398e-10	5	0.68419	Yes
19	2.3542e-10	-8.1514e-11	5.337e-10	6	1.0815	Yes
20	6.8299e-10	8.4604e-11	1.563e-09	6	1.0255	Yes
21	2.6765e-11	3.7184e-10	3.0878e-10	5	0.77587	Yes
22	-2.6178e-11	3.7964e-10	2.8232e-10	5	0.64402	Yes
23	1.3129e-10	4.2631e-10	3.8926e-10	5	0.68754	Yes
24	1.6586e-11	1.3588e-10	8.1983e-11	6	0.81692	Yes
25	6.0672e-11	1.3267e-10	1.4502e-10	5	0.68327	Yes

V. Conclusions

In this work we provided an update on the implementation of the Powered Atmospheric Landing Guidance for CALLISTO. In this case, due to the project priorities, we devoted our efforts to adapt the algorithm to the `Test Flight D`, and provided the corresponding results.

A key difference with respect to the results we shared last year is the implementation of a realistic engine model without escalating the modeling to a multi-phase approach. Instead, we proposed a simple augmentation of the system that made possible the inclusion of idle and transient modes and their time-dependency as standard look-up tables without modifying the transcription.

We showed some first results coming from nominal and dispersed simulations. The preliminary results are encouraging, although further improvements in terms of computational speed and efficiency are certainly possible: while we are writing these conclusions, the automatic generation of the flight code associated with the algorithm described here is getting completed, and ready for being tested within the actual flight processor. The corresponding processor-in-the-loop campaign, and the characterization of the performance of the algorithm in conditions closer to the flight ones will tell us exactly to what extent these improvements in terms of computational efficiency will be required.

Further activities will involve a larger Monte-Carlo campaign, both in terms of number of runs and in terms of amplitude of errors considered. Moreover, we plan to run a dedicated divert analysis, aiming at testing and verifying the behavior of the algorithm when it is effectively not possible to land at the prescribed target position. Finally, we plan to complete the integration of the landing guidance algorithm within the 6-degree-of-freedom, high-fidelity CALLISTO simulator, and to analyze its interaction with the landing controller. This activity has already been successfully performed as a stand-alone test for the `Test Flight E`, but was stopped due to the aforementioned prioritization of the project towards the completion of the analysis for `Test Flight D`, and its reprise is expected to happen in the first three months of 2025.

Acknowledgments

The first author thanks the Japanese Aerospace Exploration Agency for the long hosting started in 2018, and ending in May 2025 in the context of the CALLISTO activity, especially Dr. Shinji Ishimoto, and Dr. Taro Tsukamoto for their valuable and continuous support. Moreover, he thanks the German Aerospace Center for the special funding provided during the first 5 years of secondment.

This work has been funded by the Space Research and Development program of DLR. Its implementation will be supported by the Federal Ministry for Economic Affairs and Climate Action on the basis of a decision of the German Bundestag.

References

[1] space.com, "How many rockets has SpaceX launched in 2024?" , 2024. URL `https://spaceexplored.com/spacex-launches-2024/#:~:text=Keep%20track%20below%20of%20all%20of%20SpaceX's%202024%20launches.&text=%3C%202023-,How%20many%20rockets%20has%20SpaceX%20launched%20in%202024%3F,Falcon%20Heavy%2C%20and%20three%20Starships.`

[2] space.com, "SpaceX catches giant Starship booster with 'Chopsticks' on historic Flight 5 rocket launch and landing," , 2024. URL `https://www.space.com/spacex-starship-flight-5-launch-super-heavy-booster-catch-success-video`.

[3] Youtube.com, "China's Zhuque-3 Reusable Rocket Completes 10 Km Vertical Takeoff, Landing Test," , 2024. URL `https://www.youtube.com/watch?v=uZ2T5CKJi4s`.

[4] Japan Aerospace Exploration Agency, "Reusable Rocket Vehicle Test (RVT)," , 2001. URL `https://www.isas.jaxa.jp/e/snews/2001/06_01.shtml`.

[5] Sagliano, M., Dumke, M., and Theil, S., "Simulations and Flight Tests of a New Nonlinear Controller for the EAGLE Lander," *Journal of Spacecraft and Rockets*, Vol. 56, No. 1, 2019, pp. 259–272. https://doi.org/10.2514/1.a34161.

[6] Rmili, B., Monchaux, D., Boisneau, O., Hassin, J., Querry, S., Besson, S., Poirey, G., Bore, R., Hamada, I., Amrouchi, H., Franc, J., Barreau, M., Mercadie, N., Labois, T., and Grinco, D., "FROG, a Rocket for GNC demonstrations: Firsts flights attempts of the FROG turbojet version and preparation of the future mono-propellant rocket engine," 2019. https://doi.org/10.13009/EUCASS2019-197.

[7] Neculaescu, A.-M., Marin, A., Toader, A., Persinaru, A.-G., Cismilianu, A.-M., Tudose, M., Munteanu, C.-E., Popescu, I., Strauch, H., and Dussy, S., "System Identification and Testing for a VTVL vehicle," 2019. https://doi.org/10.13009/EUCASS2019-925.

[8] Sagliano, M., Heidecker, A., Hernández, J. M., Farì, S., Schlotterer, M., Woicke, S., Seelbinder, D., and Dumont, E., "Onboard Guidance for Reusable Rockets: Aerodynamic Descent and Powered Landing," *AIAA Scitech 2021 Forum*, American Institute of Aeronautics and Astronautics, 2021. https://doi.org/10.2514/6.2021-0862.

[9] Malyuta, D., and Açıkmeşe, B., "Fast Homotopy for Spacecraft Rendezvous Trajectory Optimization with Discrete Logic," *Journal of Guidance, Control, and Dynamics*, Vol. 46, No. 7, 2023, pp. 1262–1279. https://doi.org/10.2514/1.g006295.

[10] Sagliano, M., Seelbinder, D., Theil, S., and Lu, P., "Six-Degree-of-Freedom Rocket Landing Optimization via Augmented Convex–Concave Decomposition," *Journal of Guidance, Control, and Dynamics*, 2023. https://doi.org/10.2514/1.G007570.

[11] Sagliano, M., Hernández, J. A. M., Farì, S., Heidecker, A., Schlotterer, M., Woicke, S., Seelbinder, D., Krummen, S., and Dumont, E., "Unified-Loop Structured H-Infinity Control for Aerodynamic Steering of Reusable Rockets," *Journal of Guidance, Control, and Dynamics*, Vol. 46, No. 5, 2023, pp. 815–837. https://doi.org/10.2514/1.G007077.

[12] Sagliano, M., Seelbinder, D., Theil, S., Im, S., Lee, J., and Lee, K., "Booster Dispersion Area Management through Aerodynamic Guidance and Control," *AIAA SCITECH 2022 Forum*, American Institute of Aeronautics and Astronautics, San Diego, CA & Virtual, 2022. https://doi.org/10.2514/6.2022-0759.

[13] Lee, S.-D., and Lee, C.-H., "Multi-Phase and Dual Aero/Propulsive Rocket Landing Guidance using Successive Convex Programming," *Proceedings of the Institution of Mechanical Engineers, Part G: Journal of Aerospace Engineering*, Vol. 237, No. 8, 2022, pp. 1816–1834. https://doi.org/10.1177/09544100221138350.

[14] De Oliveira, A., and Lavagna, M., "Coupling of Advanced Guidance and Robust Control for the Descent and Precise Landing of Reusable Launchers," *Aerospace*, Vol. 11, No. 11, 2024, p. 914. https://doi.org/10.3390/aerospace11110914.

[15] Simplício, P., Marcos, A., and Bennani, S., "Reusable Launchers: Development of a Coupled Flight Mechanics, Guidance, and Control Benchmark," *Journal of Spacecraft and Rockets*, Vol. 57, No. 1, 2020, pp. 74–89. https://doi.org/10.2514/1.a34429.

[16] De Oliveira, A., and Lavagna, M., "Development of a Controlled Dynamics Simulator for Reusable Launcher Descent and Precise Landing," *Aerospace*, Vol. 10, No. 12, 2023, pp. 993–1022. https://doi.org/10.3390/aerospace10120993.

[17] Guédron, S., Ishimoto, S., Dumont, E., Tatiossian, P., Chavagnac, C., Desmariaux, J., Monchaux, D., Frenoy, O., Moreno, E. C., Deremaux, C., Lidon, N., Cesco, N., Witte, L., Sagliano, M., Seelbinder, D., Klevanski, J., Ecker, T., Reimann, B., Riehmer, J., Ertl, M., and Krummen, S., "CALLISTO DEMONSTRATOR: Focus on system aspects," *71th International Astronautical Congress, Dubai, UAE*, , No. IAC-20-D2.6.1, 2021.

[18] Acikmese, B., and Ploen, S. R., "Convex Programming Approach to Powered Descent Guidance for Mars Landing," *Journal of Guidance, Control, and Dynamics*, Vol. 30, No. 5, 2007, pp. 1353–1366. https://doi.org/10.2514/1.27553.

[19] Lu, P., "Propellant-Optimal Powered Descent Guidance," *Journal of Guidance, Control, and Dynamics*, Vol. 41, No. 4, 2018, pp. 813–826. https://doi.org/10.2514/1.g003243.

[20] Spada, F., Sagliano, M., and Topputo, F., "Direct–Indirect Hybrid Strategy for Optimal Powered Descent and Landing," *Journal of Spacecraft and Rockets*, Vol. 60, No. 6, 2023, pp. 1787–1804. https://doi.org/10.2514/1.A35650, URL https://doi.org/10.2514/1.A35650.

[21] Liu, X., "Fuel-Optimal Rocket Landing with Aerodynamic Controls," *Journal of Guidance, Control, and Dynamics*, Vol. 42, No. 1, 2019, pp. 65–77. https://doi.org/10.2514/1.g003537.

[22] Davami, C., Lu, P., and Johnson B., A. J., Rosengren, "Optimizing End-to-End EDL Trajectories for High-Mass Mars Landings," *2024 AAS/AIAA Astrodynamics Specialist Conference*, American Astronautical Society (AAS), 2024.

[23] Szmuk, M., Acikmese, B., and Berning, A. W., "Successive Convexification for Fuel-Optimal Powered Landing with Aerodynamic Drag and Non-Convex Constraints," *AIAA Guidance, Navigation, and Control Conference*, American Institute of Aeronautics and Astronautics, 2016. https://doi.org/10.2514/6.2016-0378.

[24] Jung, C.-G., Kim, B., Jung, K.-W., and Lee, C.-H., "Thrust Integrated Trajectory Optimization for Multipulse Rocket Missiles Using Convex Programming," *Journal of Spacecraft and Rockets*, Vol. 60, No. 3, 2023, pp. 957–971. https://doi.org/10.2514/1.a35524.

[25] Lu, P., and Davami, C., "Rethinking Propellant-Optimal Powered Descent Guidance," *Journal of Guidance, Control, and Dynamics*, Vol. 47, No. 10, 2024, pp. 2016–2028. https://doi.org/10.2514/1.g008343.

[26] Wang, Z., and Grant, M. J., "Optimization of Minimum-Time Low-Thrust Transfers Using Convex Programming," *Journal of Spacecraft and Rockets*, Vol. 55, No. 3, 2018, pp. 586–598. https://doi.org/10.2514/1.a33995.

[27] Sagliano, M., and Mooij, E., "Optimal drag-energy entry guidance via pseudospectral convex optimization," *Aerospace Science and Technology*, Vol. 117, 2021, p. 106946. https://doi.org/10.1016/j.ast.2021.106946.

[28] Hofmann, C., Morelli, A. C., and Topputo, F., "Performance Assessment of Convex Low-Thrust Trajectory Optimization Methods," *Journal of Spacecraft and Rockets*, Vol. 60, No. 1, 2023, pp. 299–314. https://doi.org/10.2514/1.a35461.

[29] Hofmann, C., and Topputo, F., "Convex Low-Thrust Trajectory Optimization with No-Thrust Constraints and Moving Target," *Journal of Spacecraft and Rockets*, 2024, pp. 1–11. https://doi.org/10.2514/1.a35877.

[30] Zhao, J., Li, J., and Li, S., "Low-Thrust Transfer Orbit Optimization Using Sequential Convex Programming and Adaptive Mesh Refinement," *Journal of Spacecraft and Rockets*, 2023, pp. 1–18. https://doi.org/10.2514/1.a35817.

[31] Zhao, Z., Shang, H., Liu, C., and Xiao, S., "Mesh-Based Two-Step Convex Optimization for Spacecraft Landing Trajectory Planning on Irregular Asteroid," *Journal of Spacecraft and Rockets*, Vol. 61, No. 1, 2024, pp. 72–87. https://doi.org/10.2514/1.a35715.

[32] Szmuk, M., Reynolds, T. P., and Açıkmeşe, B., "Successive Convexification for Real-Time Six-Degree-of-Freedom Powered Descent Guidance with State-Triggered Constraints," *Journal of Guidance, Control, and Dynamics*, Vol. 43, No. 8, 2020, pp. 1399–1413. https://doi.org/10.2514/1.g004549.

[33] Lee, S.-D., Jung, K.-W., and Lee, C.-H., "Mission Profile Analysis of Point-to-Point Rocket Cargo Transportation System Using Trajectory Optimization," *Journal of Spacecraft and Rockets*, Vol. 61, No. 1, 2024, pp. 263–273. https://doi.org/10.2514/1.a35766.

[34] Liu, X., Li, S., and Xin, M., "Mars Entry Trajectory Planning with Range Discretization and Successive Convexification," *Journal of Guidance, Control, and Dynamics*, Vol. 45, No. 4, 2022, pp. 755–763. https://doi.org/10.2514/1.g006237.

[35] Sagliano, M., Heidecker, A., Farì, S., Alfredo, M. H. J., Schlotterer, M., Woicke, S., Seelbinder, D., and Dumont, E., *Powered Atmospheric Landing Guidance for Reusable Rockets: the CALLISTO studies*, 2024. https://doi.org/10.2514/6.2024-1761, URL https://arc.aiaa.org/doi/abs/10.2514/6.2024-1761.

[36] Dumont, E., Ishimoto, S., Illig, M., Sagliano, M., Solari, M., Ecker, T., Martens, H., Krummen, S., Desmariaux, J., Saito, Y., Ertl, M., Klevanski, J., Reimann, B., Woicke, S., Schwarz, R., Seelbinder, D., Markgraf, M., Riehmer, J., Braun, B., and Acher, M., "CALLISTO: Towards Reusability of a Rocket Stage: Current Status," *Journal of Evolving Space Activities*, Vol. 1, 2023, p. 75. https://doi.org/10.57350/jesa.75.

[37] ISO Central Secretary, "Flight Dynamics - Concepts, quantities and symbols, ISO 1151-1," Standard ISO 1151-1:1988, International Organization for Standardization, 1988. URL https://www.iso.org/standard/5699.html.

[38] Salguero, D. E., "Trajectory Analysis and Optimization," Tech. rep., Sandia National Laboratories, 1995.

[39] Platus, D. H., "Angle-of-attack convergence and windward- meridian rotation rate of rolling re-entry vehicles," *AIAA Journal*, Vol. 7, No. 12, 1969, pp. 2324–2330. https://doi.org/10.2514/3.5535.

[40] Ecker, T., Ertl, M., Klevanski, J., Krummen, S., and Dumont, E., "Aerothermal characterization of the CALLISTO vehicle during descent," *CEAS Space Journal*, 2024. https://doi.org/10.1007/s12567-024-00561-z.

[41] Domahidi, A., Chu, E., and Boyd, S., "ECOS: An SOCP solver for embedded systems," *2013 European Control Conference (ECC)*, IEEE, 2013. https://doi.org/10.23919/ecc.2013.6669541.